DTIC FILE COPY

(2)

AD-A220 089

N00014-89-C-0226

FINAL REPORT
SBIR N 00014 89 C0226

NOVEL ACOUSTIC DAMPING MATERIALS

1989

MEMRY CORP
83 KEELER AVE
NORWALK, CT 06854

DTIC
ELECTE
MAR 30 1990
S B D

DISTRIBUTION STATEMENT A
Approved for public release
Distribution Unlimited

90 03 27 074

TABLE OF CONTENTS

QUALITY INSPECTED 4

Accession For
NTIS GRA&I
DTIC TAB
Unannounced
Justification
By per telecon
Distribution/
Availability Codes
Dist | Avail and/or Special
A-1

STATEMENT "A" per Donald Polk
ONR/Code 11SP
TELECON 3/28/90

VG

NOVEL ACOUSTIC DAMPING MATERIALS

INTRODUCTION:

The terms 'smart' or 'intelligent' materials appear in the technical literature with increasing frequency and more recently a new international journal devoted to this subject has been announced, The Journal of Intelligent Material Systems and Structures. The concept basic to these new materials is that sensors and actuators of various types can be incorporated in or attached to plates, beams, shells and similar structural members and provide either information on the integrity of the component in its service environment or through some external activation modify the properties of the member in some beneficial manner. In the former mode of operation, the sensor might be a piezcelectric or shape memory element or a fiber optic device which would provide early detection of a fatigue derived defect or the onset of some structural change which could ultimately impair the performance of the structure. Used as an active element in the structure the modal response, acoustic radiation or transmission can be modified as well as the internal damping or suppression of vibration. The major attention being given to this new class of material is in the field of composites where the opportunity to design into the structure a wide variety of properties is possible. At the present time the emphasis has been on fiber reenforced plastics such as glass-epoxy and graphite-epoxy composites which are broadly used in aircraft and aerospace structures.

Noise and vibration in structures range in impact from annoyance and discomfort to passengers in various transportation systems to severe limitation of the component life. In aerospace systems the requirements of function and launching lead to lightweight and slender components which are vulnerable to fatigue failure due to low damping. Rotating machinery such as jet engines are designed to minimize the ratio of vibratory to steady state stress. Any increase in vibratory stress reduces the allowable steady state stress which in turn requires an increase in cross section area and weight, an expensive penalty. Airborne and structurally borne noise in rotor-craft has long been a problem limiting broader commercial application of these versatile aircraft. The requirements of the next generation of space stations and space exploration vehicles place great emphasis on a vibration free environment for effective functioning of personnel, operation of gravity free processes and

for tactical requirements of repositioning the craft where its function is military in nature. The Navy has a broad mandate for reducing noise in surface and undersea vessels which has lead to extensive research on methods for controlling noise radiation as well as to isolate or damp vibrations at the source.

In all of the situations mentioned the traditional solution is to consider the inter-relation between structural design, material characteristics and aerodynamic damping and to design the structure based on an estimate of these interactions. This invariably leads to an increase in stiffness of the component resulting in increased weight and cost. Structural alloys possess very little damping, and estimates of structural damping arising out of rubbing at joints have essentially defied all attempts at accurate measurement and analysis. In a similar vein, the calculation of aerodynamic damping has yielded results which are often at variance with observation.

In the light of the broad requirements listed above the study of composite materials which combine structural performance with active or passive vibration and acoustic control should be given a high priority.

The application of intelligent composites can be divided into a number of generic areas; for example:

Heat Activated Actuators
Electrically Activated Actuators
High Damping Applications
Variable Geometry for Modal Response Shift
Variable Geometry for Assembly/Maintenance
High Plastic Strain Applications

In order to establish the feasibility of exploiting intelligent composites a great deal of design data is required, both theoretical as well as experimental. Included in such a data list would be:

Density
Static Strength
Fatigue Strength
Operating Temperature and Range
Repeatability
Acoustic
Frequency Response Guidelines
Constitutive Relations for
  Sensor/Actuator Materials
Power Consumption
Cost
Design Methodology Handbook

In the proposed research program the choice of composite material was graphite-epoxy imbedded with nickel-titanium shape memory alloy wires. The choice was made based on the capabilities of the United Technology Research Laboratory facilities to produce the required test specimens and the availability of a shape memory alloy with the required transformation temperatures and the required wire

sizes. The realizable objectives of the program were established after conference involving United Technology specialists in composites and in the field of applied mechanics and vibration and the engineering staff of Memry Corp. These objectives were as follows:

1. Characterization of the Nickel-Titanium shape memory alloy
2. Fabrication of graphite-epoxy composite specimen with imbedded shape memory wires of various transformation characteristics and in various volume percentages.
3. Perform damping measurements using FFT analysis of the output of a resonance dwell apparatus.
4. Determine mechanical properties of the composite assemblies.
5. Assess the potential of these intelligent composites for vibration and acoustic control and outline suggestions for a Phase II efforts.

EXPERIMENTAL PROCEDURES

The measurement of damping is accomplished by a wide variety of techniques using specimen in the form of wire, rod, sheet or plate and strip. Some of these forms provide information on the changes in modal response brought about by shifts in damping characteristics or changes in the elastic modulus or stress states of the specimen. Measurements on plate vibration is typical of this type of measurement. Where damping as a function of stress is of interest, torsion or cantilever specimen tests are usually exploited. Most of the systems can in some way accommodate an environmental chamber to allow damping measurements to be performed over a range of temperatures. In some cases, the elimination of air damping is important, thus requiring measurements in vacuum. Taking into consideration the limited time period available, the desirability of measuring damping as a function of stress, and the type of specimen most readily fabricated by the United technology Research Laboratory personnel the resonance dwell damping apparatus was chosen for damping measurements. This apparatus was designed by the well known acoustic engineering firm Bolt Beranek and Newman Inc. for material damping studies, and has been used by the Naval Post Graduate School research group in their studies of the damping of copper-manganese alloys and of various shape memory alloys. It lends itself to studies of damping as a function of stress, and, although not used in the present study, can be readily fitted with a temperature controlled specimen chamber and or a vacuum chamber.

The single cantilever beam resonance dwell apparatus is used to determine the stress and frequency dependence of material damping at engineering stress levels in the frequency range from 25 to 100 Hz. The resonance dwell technique is a forced vibration method of indirectly determining the loss factors of simple structural elements by measuring their response to excitation at a modal frequency. For a thin beam, where the modes and dynamic stress distributions are well known, the specific damping capacity of the material, defined as the energy dissipated per unit volume in one stress cycle at a given peak stress divided by 2π times the peak potential energy in the unit volume at the same stress, may be inferred from the determined loss factor. In the resonance dwell test the specimen loss factor, g_s, in a mode, usually the fundamental, is derived from the resonance amplification factor Q of the specimen in that mode. The mechanical Q of a vibrating system is defined in terms of a characteristic deflection δ of the system due to the distributed exciting forces proportional to the inertia forces of the mode in question; thus, the amplification factor at resonance is:

$$Q = \frac{\delta_{res}}{\delta_0}$$

where δ_0, is the deflection due to the distributed exciting force being applied statically and δ_{res} is the deflection when the same pattern of forces is applied in simple harmonic motion at the modal natural frequency. The relationship between Q, the specimen loss factor g_s, and the logarithmic decrement ζ of a single-degree-of-freedom system is:

$$\zeta = \frac{\pi}{Q} = \pi g_s$$

The advantages of the resonance-dwell method are: first, the ratio of δ_0/δ_{res}, for a properly designed specimen, is dependent only upon the damping in the specimen; second, the vibration amplitude δ_{res} may be maintained at any constant level so that specimen damping may be determined as an increasing function of stress, eliminating the possibility of stress history effects; and third, because nothing is attached directly to the vibrating specimen, extraneous energy losses are minimized. The latter was specific to the use of an optical technique to measure the vibrating tip amplitude, however the use of very small strain gauges with find lead wires is equivalent in performance.

The method for ensuring that the beam specimen is excited at a mode is straightforward. The apparatus is constructed in such a way that the specimen acts as a vibration absorber placed in a single degree-of-freedom supporting system. At a natural frequency of the

beam, the response of the supporting system is minimized. The frequency of the response minimum, and hence of the beam mode, can therefore be determined by monitoring the acceleration of the supporting system.

As we pointed out above, in its original, form the amplitude of vibration of the cantilever beam was measured using an optical measurement of the tip amplitude. This was facilitated by illuminating the tip with a stroboscopic light which gave a "stationary" image to sight on through the measuring telescope. This is an acceptable technique when measuring damping on a homogeneous material where, knowing the elastic modulus, one can calculate the mean and maximum root stress of the vibrating specimen. In the case of the composites being evaluated, with their variety of shape memory wire volume content, an alternative measurement of specimen stress was required. Strain gauges were affixed to the root surface of the cantilever specimen and the output of a strain gage bridge could be either read directly or used as the input to a FFT vibration analyzer with the recorded output indicated as microstrain.

The resonance dwell apparatus shown in Fig. 1 consists of a massive steel frame on which is mounted a flexure plate holding the specimen. The flexure specimen support is in turn driven by an electromagnetic shaker excited by a variable frequency oscillator whose output is amplified by a high quality audio amplifier. The acceleration imparted to the specimen is measured by an accelerometer placed on the flexure at a point close to the specimen root.

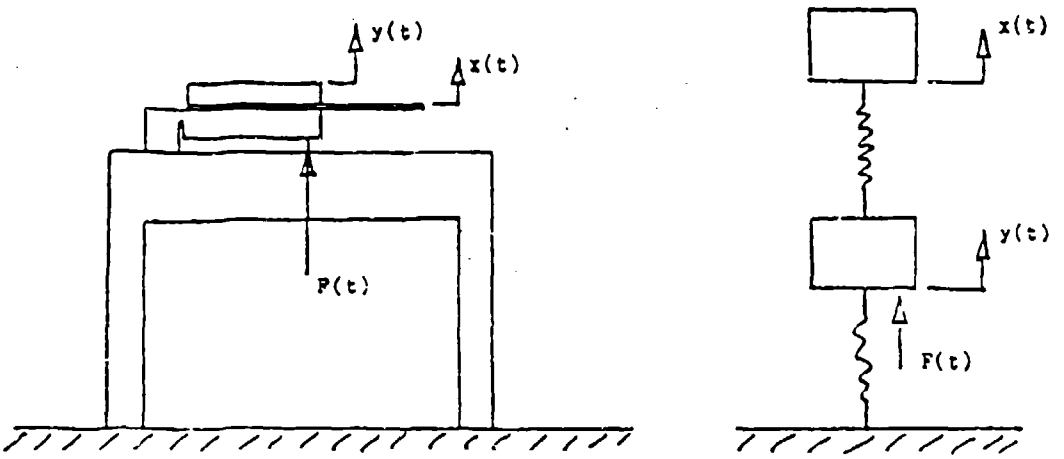

Figure 1.
The Resonance Dwell Damping Apparatus is the Equivalent of an excited System with a Resonant Vibration Absorber

Computational Methods:

The calculation of specimen loss factor can be carried from the measured double tip amplitude of the specimen when excited at its fundamental mode and the value of the root acceleration a_o. For these measured values to be valid the specimen must be vibrating at its fundamental mode; achieved by sweeping the variable oscillator slowly upward while monitoring the root acceleration. The natural frequency of the specimen is that frequency at which the sharp minimum or "notch" in acceleration occurs. Although, as mentioned earlier, the double tip amplitude was measured optically, for the composite specimen the root strain was converted to root stress and from this value the tip amplitude was calculated. The loss factor g_s is related to the root acceleration a_o, the fundamental frequency f_1, and the beam tip double amplitude $y_{t,DA}$, by the equation:

$$g_s = 0.083[1+0.2L]\frac{a_o}{f_n^2}\frac{1}{y_{t,DA}} \qquad \text{(1) BBN \#3}$$

The material specific damping capacity may then be calculated for each stress level from the specimen loss factor by:

$$C_1(\sigma,\omega) = \frac{g_s(\sigma,\omega)}{R_1} \qquad \text{(2) BBN\#4}$$

where

$$R_1 = \left[\frac{3}{n+3}\right]2^{-n}\frac{\int_0^{\lambda}\phi_1^{n+2}(z)\,dz}{\int_0^{\lambda}\phi_1^2(z)\,dz} \qquad \text{(3)BBN\#5a}$$

$$\phi_1(z) = \cosh Z+\cos Z-\beta[\sinh z+\sin z] \qquad \text{(4)BBN\#5b}$$

$$\beta_1 = \frac{\cosh\lambda+\cos\lambda}{\sinh\lambda+\sin\lambda} \qquad \text{(5)BBN\#5c}$$

and $\lambda = 1.8751$

A full development of the measurement and calculation methodology ror the resonance dwell technique is given in Appendix A.

Material Loss Factor:

Material loss Factor is evaluated for the "Blank" unmodified graphite-epoxy specimen and for the F2015-020 specimen which contains 0.020" diametere NiTi wires near the outermost specimen surface, constituting 10.9% of the total volume. Of the specimens examined, the F2015-020, in which the NiTi is martensitic, is the only one which exhibited a significant level of damping. The specimen loss factor vs strain plots are shown in Figures 2 and 3 for the blank and the F2015-020 specimen. From these plots can be determined the specimen loss strain exponent n since:

$$\text{Log}_{10}[g_s] = n \log_{10}[\sigma] - k$$

A. "Blank"

First Microstrain Range $700<\mu\epsilon<280$, n = 1.000
Second Microstrain Range $280<\mu\epsilon<1000$, n = 0.716

B. F2015-020 #2

Microstrain Range $53<\mu\epsilon<1000$, n = 0.547

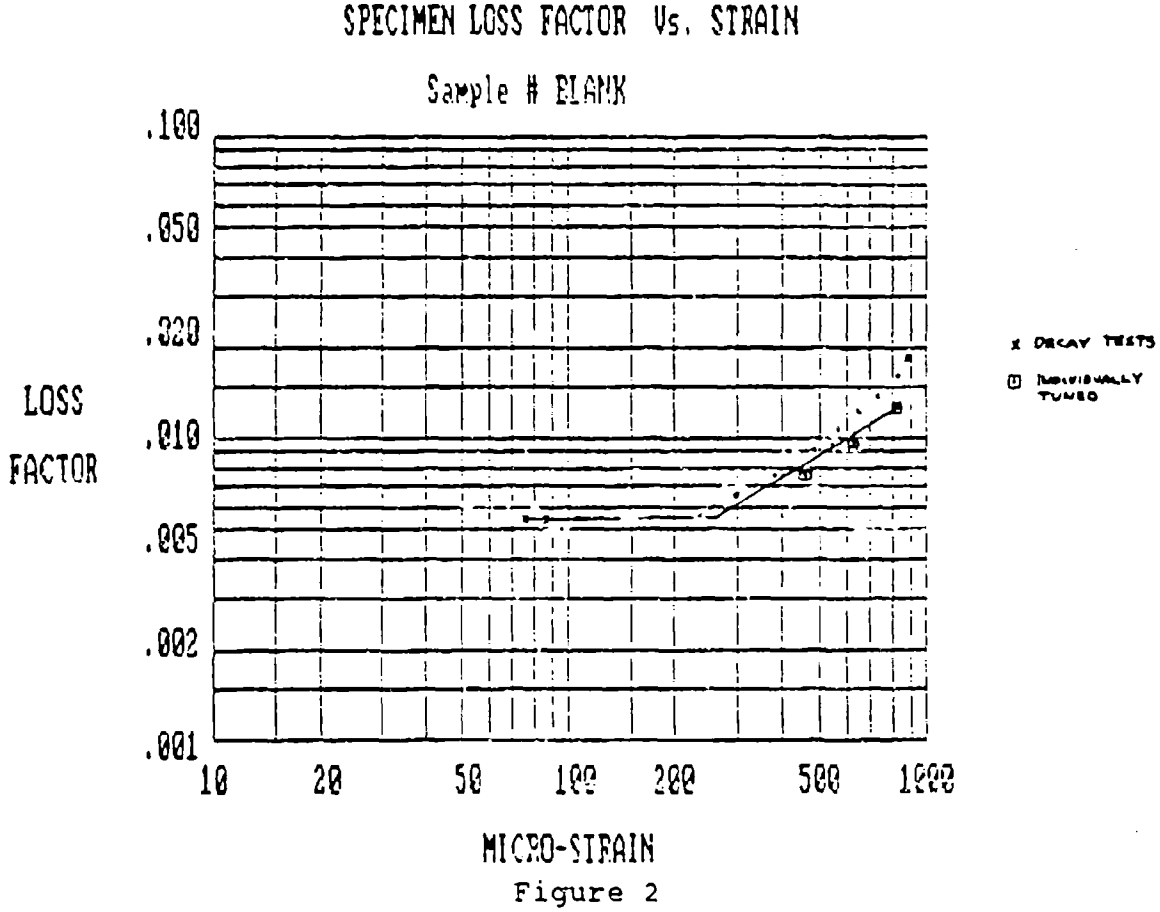

Figure 2

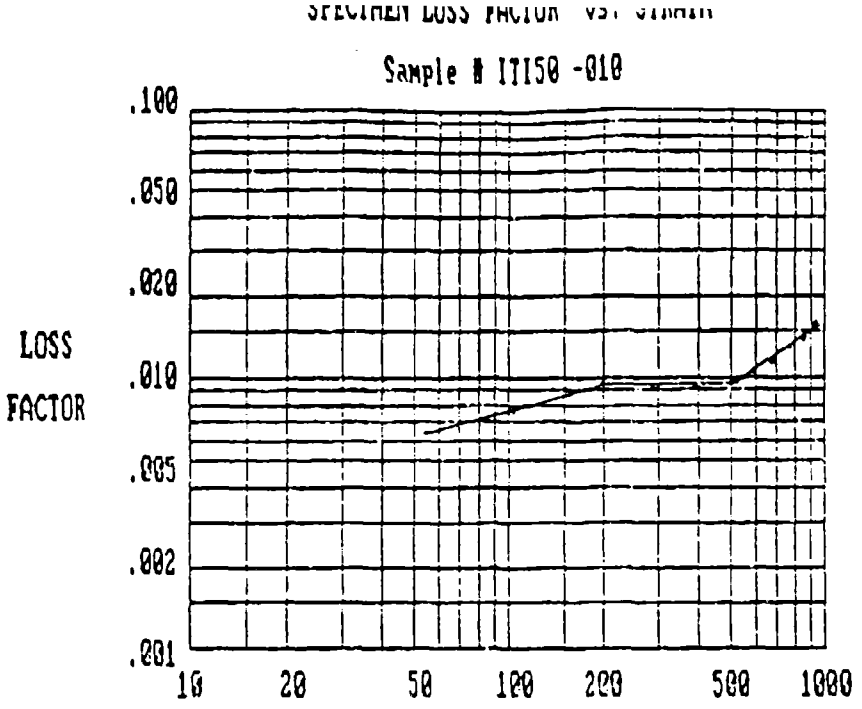

Figure 3

Figures 4 and 5 show loss factor vs log strain for two specimen which contain NiTi in the beta phase where it would behave in a superelastic manner.

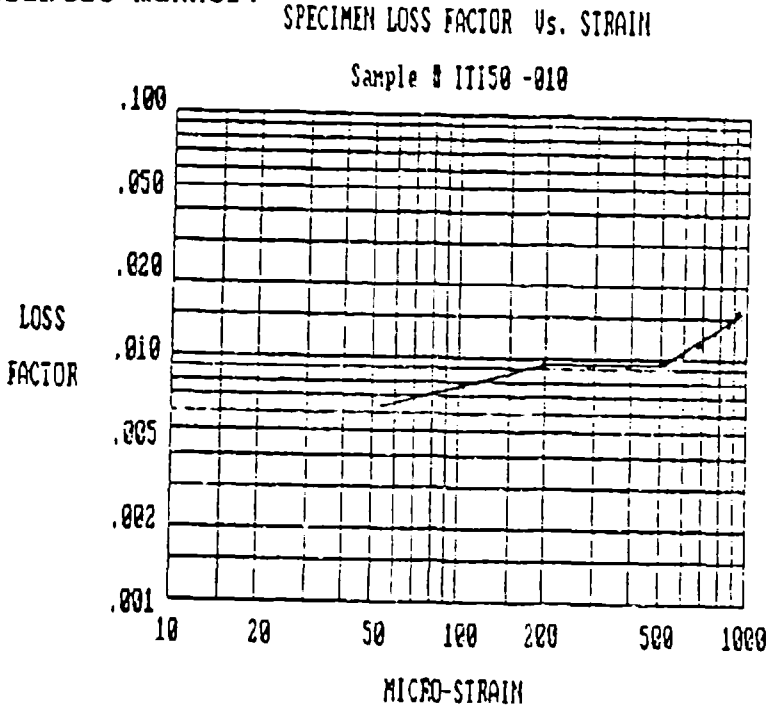

Figure 4

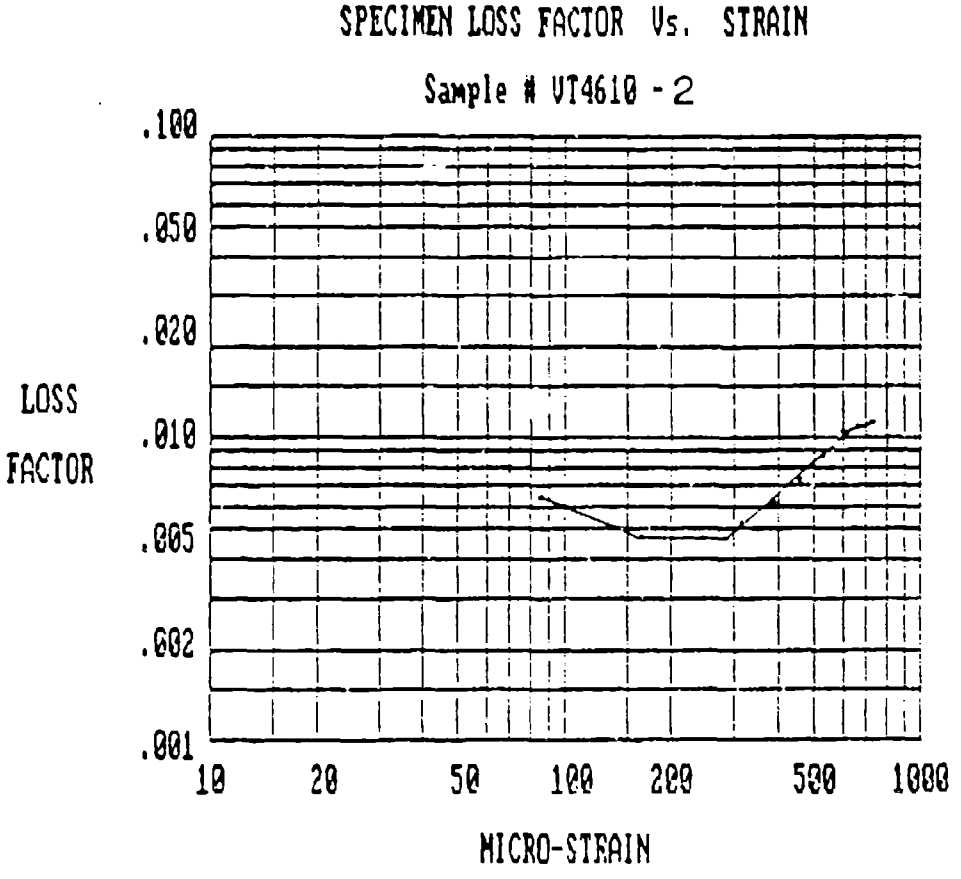

Figure 5

For A.1 where n ≡ 1.000 the material to specimen loss factor ratio is =1.000. For values of n ≠ 1 the strain dependent energy loss must be integrated over the strain field, see Equations 28,40 and 41, as well as 42-51 in appendix A. The integration of the strain energy:

$$\int_0^{\lambda} Q_1(z)\,dz$$

may be carried out in closed form and yields:

$$\int_0^{\lambda} Q_1^2(z)\,dz = \lambda + \frac{1}{4}(sin2\lambda + sinh2\lambda) + \frac{1}{4}C^2(sinh2\lambda - sin2\lambda) + (C^2+1)\sin\lambda\cosh\lambda$$

$$+(1-C^2)\cos\lambda\sinh\lambda - C(\sin^2\lambda + \sinh^2\lambda) - 2C\sin\lambda\sinh\lambda$$

where C = 1/T, see equation 43, Appendix A

and for λ = 1.8251

$$\int_0^{1.8751} Q^2(z)\,dz = 1.8751$$

The integration of the energy loss due to strain dependent damping

$$\int_0^{\lambda} Q^{2+n}(z)\,dz$$

on the other hand is directly intractable and the integration must be performed numerically. The evaluation is performed by Simpson's Rule in automatic fashion with a computer program and, combined with other factors, provides the evaluation of the material to specimen loss factor ratio, β/α, see equation 48 in Appendix A. These results are are given for the "Blank" specimen and for the martensitic NiTi wire specimen F2015-020-#2 using Simpson's Rule integration of Y(x) for x from 0 to L.

Blank Specimen: Loss-Strain Exponent = 0.716
β/α = 1.552671
For strain range: 280< $\mu\epsilon$ > 1000

F2015-020-#2: Loss-Strain Exponent = 0.547
β/α = 1.411618
For strain range: 53 < $\mu\epsilon$ > 1000

The material loss factor as f(strain) for the above specimens is shown graphically as log(loss factor) vs. log(micro- strain) in Figure 6.

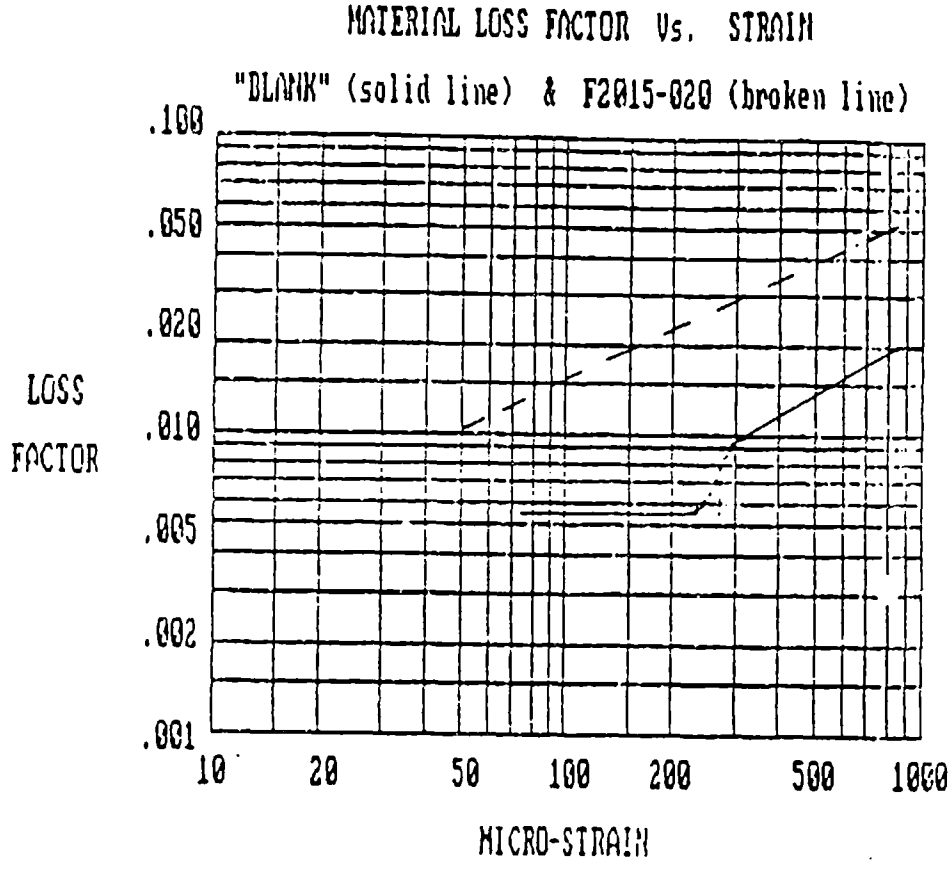

Figure 6.

SPECIMEN PREPARATION:

The selection of a composite material to be used as a matrix composition for imbedded shape memory wires was made with the consulation of the composites group of the United Technology Research Laboratory(UTRC), East Hartford, Ct. In the preparation of the Phase I proposal the UTRC was designated for specimen fabrication as well as consulting on the methodology of damping evaluation. After reviewing the facilities and capabilities of the experimental composites section of the laboratory, the technique chosen for fabrication was hot pressing, and the material formulation suggested was the Hercules Corporation pre-impregnated roving designated AS4-3501-6. The proposed method of fabrication was by hot pressing; and the typical specimen size used by UTRC is 4.5" wide by 11.5 inches long. For the cantilever specimen used in the 12olt Beranek and Newman resonance dwell apparatus, the desired specimen width is 1"; as, such, four specimen could be cut from each hot pressed sample.

Pre-preg AS4-3501-6 Hercules Unit Tape type ASI was provided by UTRC in the form of 4.5" wide by 12" long tapes 0.005" thick. The tape was refrigerated until ready for lay up. NiTi wire of four compositions were selected with the transformation characteristics

as determined by a Differential Scanning Calorimeter as shown in Figs. 7-10. On the graph is shown the onset temperature which is automatically computed by the Perkin Elmer DSC instrument as the intersection of the two slopes up the upper, martensite to beta, transformation. These values are as follows:

Specimen-Diameter	Onset Temperature °C	R.T.Structure
V4610-0.020"	10.81	Beta
ITI30-0.010"	23.36	Mart.-Beta
F2015-0.020"	40.12	Martensite
ITI50-0.010"	32.75	Martensite

The V4610 composition was for examining the potential of stress induced martensite (SIM) as a mechanism for energy absorption. The ITI30 was also to be used in that mode of operation or for observing the modulus shift in a specimen, i.e. its ist mode resonance frequency where in that case the NiTi wire is electrically heated to cause the phase transformation. The F2015 and the ITI50 are essentially martensitic at room temperature and as such were to be imbedded as passive damping wires at two levels of volume percent.

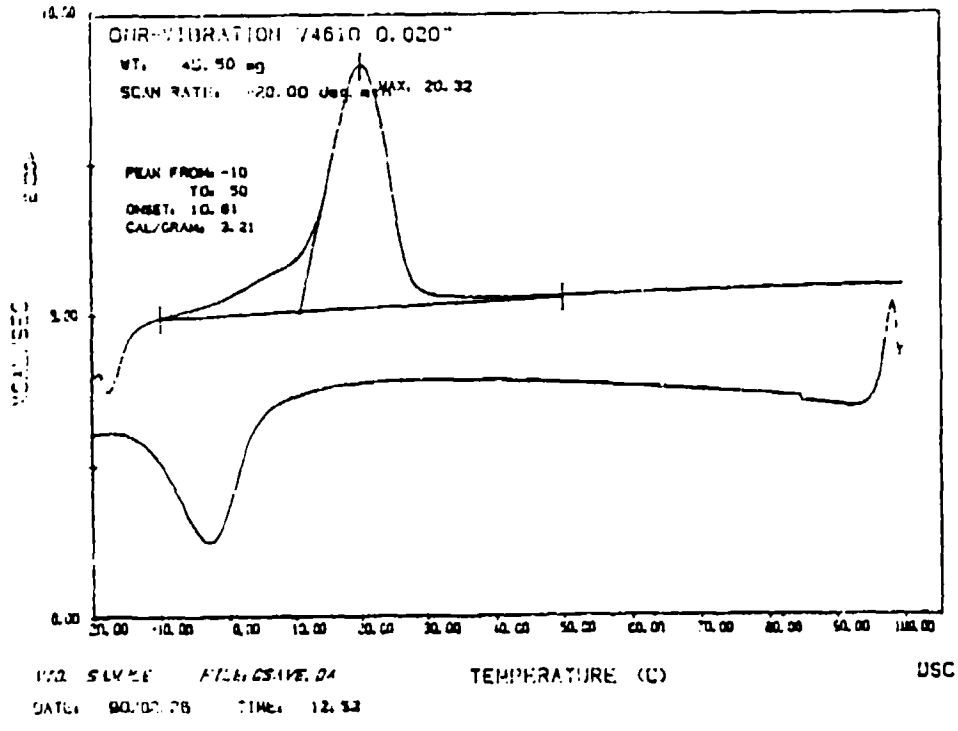

Figure 7

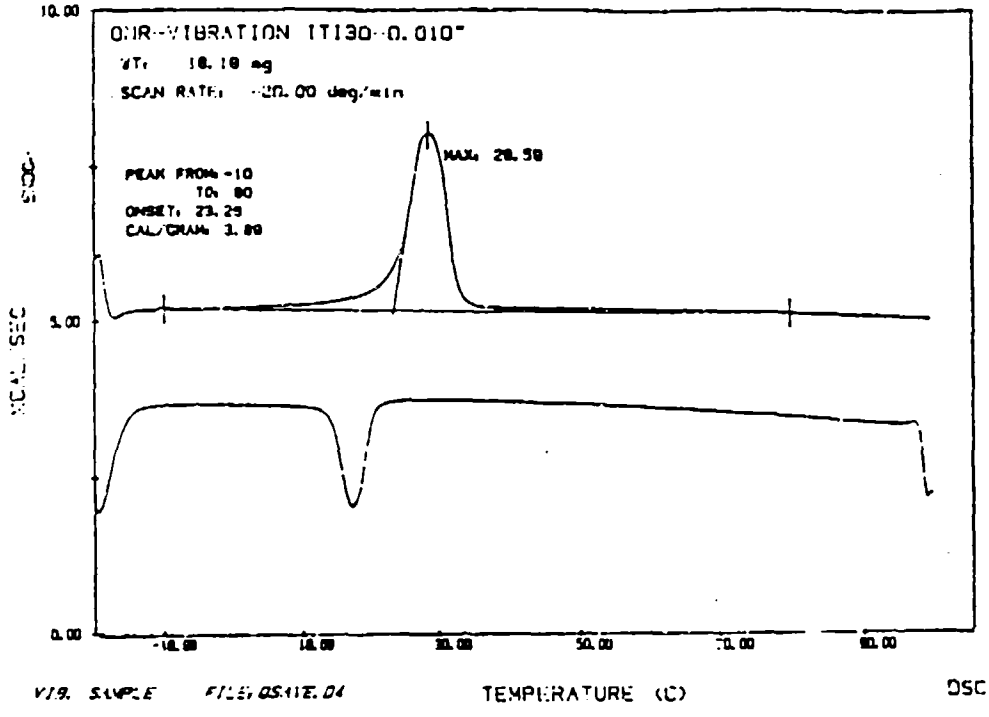

Figure 8

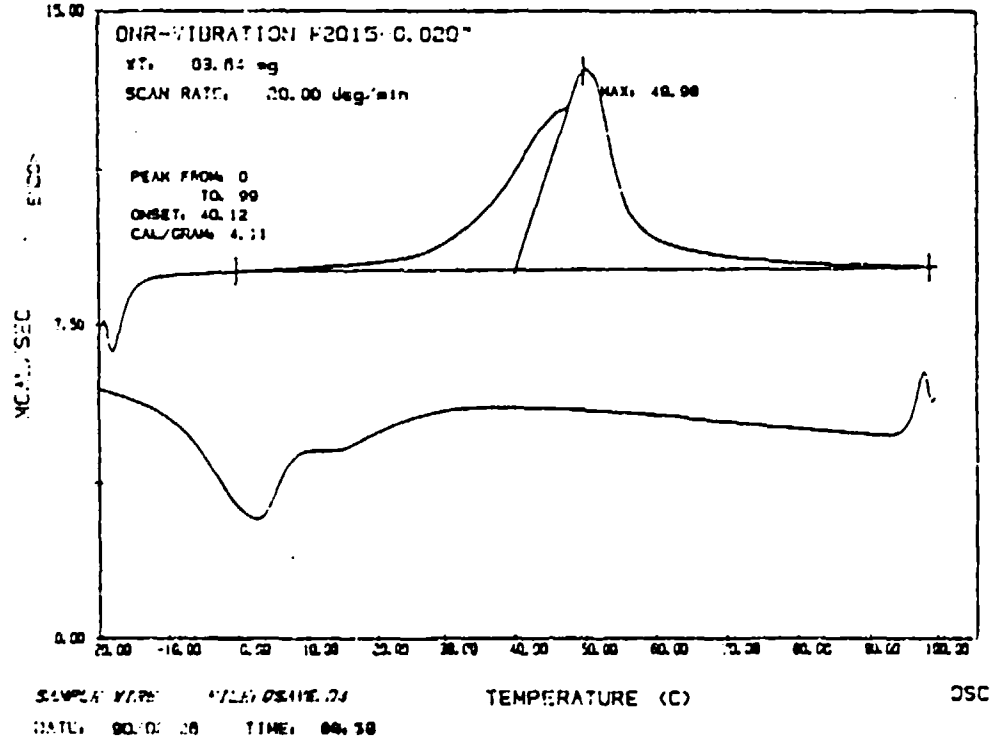

Figure 9

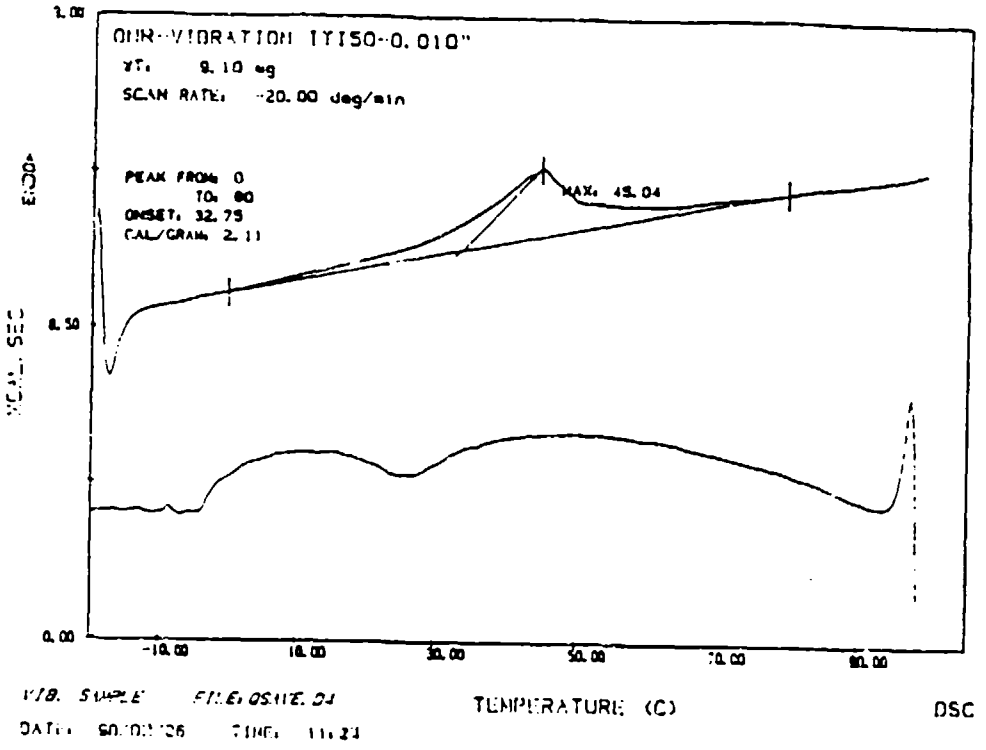

Figure 10

NiTi wire in the as drawn condition has a heavy oxide, a result of the interpass annealing. This oxide can flake off or break under wire stressing, and be a potential loss of resin-wire bond. Cleaning of the wire requires a sulfuric-hydrofloric acid dip, followed by water rinse. The lay up of the wire-graphite-pre-preg was carried out by weaving the wires on a loom which was then pressed on to the first pre-preg layer. This was followed by eighteen additional pre-preg layers, followed by another wire layer and then a final outer pre-preg layer. This package was then again refrigerated to prevent the epoxy from setting before the hot pressing. The hot pressing was carried out by UTRL at a temperature of 350°F. After curing, the nominally 4.5" wide by 11" long plates had re-enforcing ends cemented to one end. This provided a heavy end to the cantilever specimens to prevent end effects from variable gripping in the damping apparatus. After the ends had been applied the plates were longitudinally cut into 1" wide cantilever specimen using a diamond saw with a very thin kerf. The specimen prepared in this manner were then fitted with strain guages, mounted at the root as close as possible to the tip re-enforcement. The configurations of imbedded wires were as follows:

1. Blank specimen with no wires for control comparison.
2. Graphite-Epoxy with 18 0.020" dia. Martensitic wires in the two outer surfaces.
3. Graphite-epoxy with 18 0.010 dia. Martensitic wires in the two outer surfaces.
4. Graphite-epoxy with 18 0.020 dia. Beta wires in the two

outer surfaces.

5. Graphite-epoxy with one continuous strand of 0.010" dia.wire laid down in four parallel to lines with the two ends protruding for electrical attachment.

These are shown in the photographs of Figures 11-13.

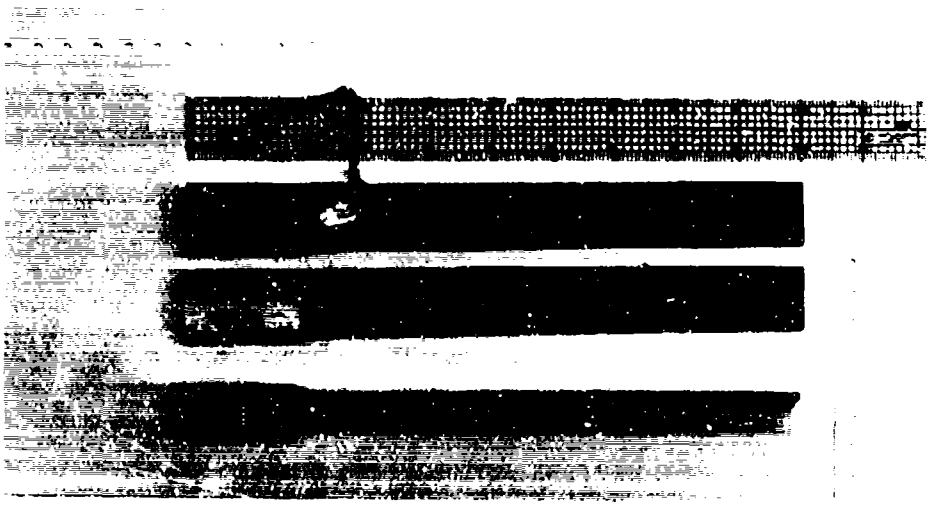

Figure 11
Top: specimen with strain gauge attached. Middle: blank. side view
Bottom: showing re-enforced tip profile.

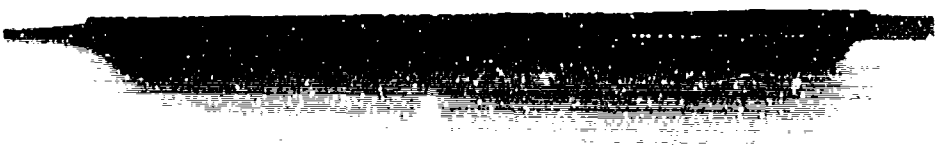

Figure 12
Cross section showing imbedded wires. Note displacement of wires as a result of the hot pressing forces.

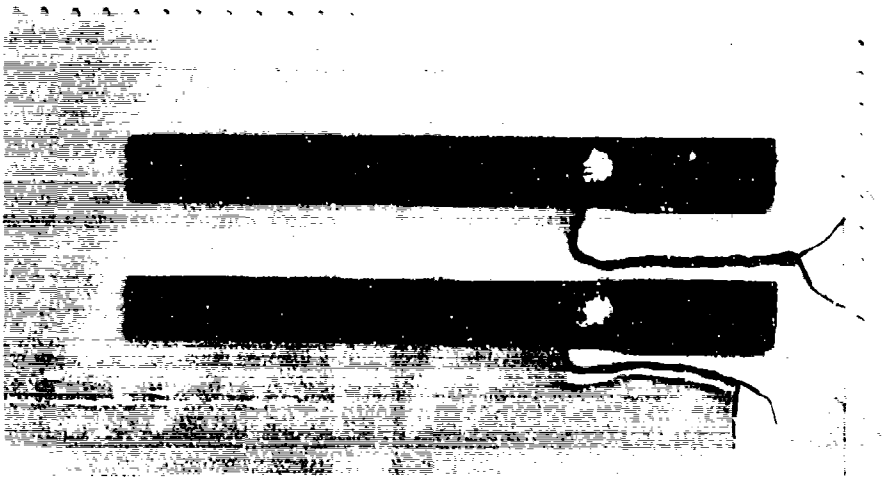

Figure 13

Two specimens with continuous loops of NiTi imbedded wires

Four duplicate specimens were fabricated from each hot pressed plate, however due to the shifting of wires during the hot pressing when the diamond saw slitting was carried out some of the wires were cut and partially detached; as such, these specimens couldn't be used. The very small strain gauges used were difficult to apply and in some cases the finished bonded unit was out of tolerance in terms of resistance, probably a result of shorting by a drop of solder. Sufficient units were available for test.

The nature of the epoxy to wire bond is difficult to estimate, although Rogers et al (1) have developed a notched specimen for determining the bond quality. Due to the very high strength of graphite-epoxy composites the full width of a cantilever specimen could not be tested. The major problem in tensile testing these materials lies in their very low friction, making adequate gripping in the tester a real problem. In Figure 14 is shown a typical test curve with the serrations due to the slippage in the grips. The blank specimens had an average peak tensile load before slipping of 92,210 psi. The published value of ultimate tensile stress for these composites is 310,000 psi at a graphite fiber loading of 62%. Specimen with imbedded wires averaged 63,500 psi with no sign of wire pull-out. It was concluded that the wire pretreatment was effective in providing good matrix to wire bonding.

Although the even spacing of the wires when mounted in their jig was not preserved in the hot pressing, for the narrow width of the cantilever the effect of this on damping is not considered to be great nor as important as the volume percentage of wires. The two volume percent levels were nominally 3% and 10% From the results it would appear that levels from 15% to 20% would have been more effective and this is borne out by subsequent reports and conversations with Prof. Craig Rogers of the Intelligent Materials group at Virginia Polytechnic Institute, Blacksburg, VA.

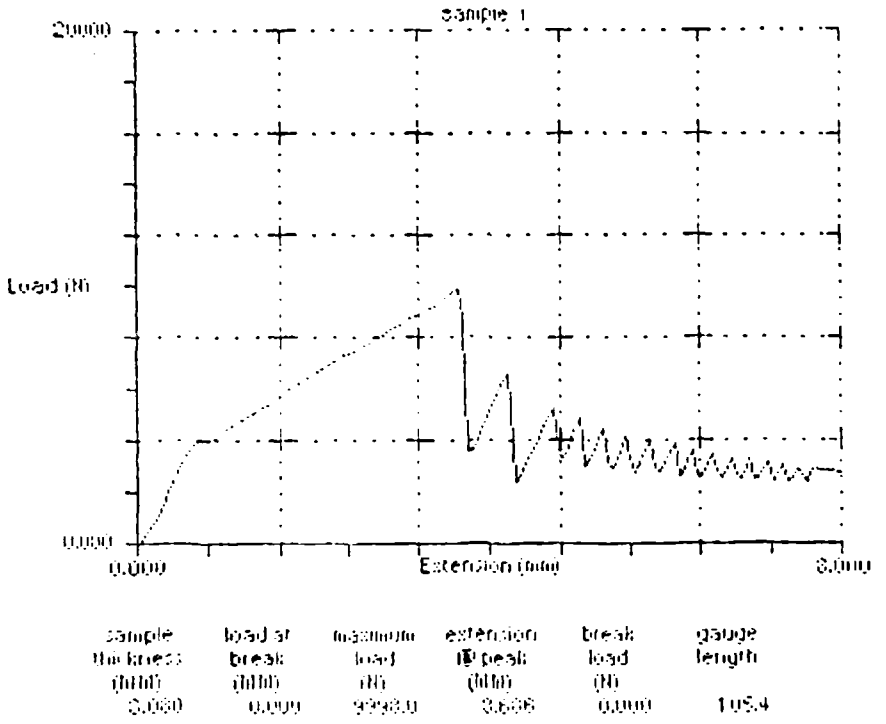

sample thickness (mm)	load at break (mm)	maximum load (N)	extension at peak (mm)	break load (N)	gauge length
3.060	0.000	[illegible]	[illegible]	0.000	105.4

Peak Load
55,636 psi

Figure 14

TESTING PROCEDURES

The resonance dwell apparatus described briefly in the discussion of computational techniques is shown in the photographs of Figures 15 and 16. The Hewlett Packard Model 204C oscillator provides the variable frequency drive to the Crown DC-300 dual 150 watt/channel amplifier which provides the excitation for the Type 409 LTV Ling Altec shaker. The close-up view of the shaker shows the accelerometer mounted on top of the specimen holder, and the connector strip which provides easy connect-disconnect for the strain gauges. The strain gauge output is fed to the Micro-Measurements Group bridge. The output from the accelerometer and the strain gauge bridge are fed to the Computational Systems Inc. Wavepak FFT signal analyses. This is a hard board system which, added to a high power PC computer, provides digital oscilloscope emulation as well as FFT Spectrum Analyzer emulation. With added software this system can also do modal analysis. The resonance dwell apparatus is shown in the photograph, Figure 15, where the components are, left to right: The Crown Amplifier, Hewlett Packard Oscillator, Amplifier output voltmemet, Strain gauge bridge and the steel frame with the specimen mount and the shaker . In Figure 16 is a close up view of the shaker showing the cantilevered specimen holder with flexure, the top mounted accelerometer and the strain gauge leads.

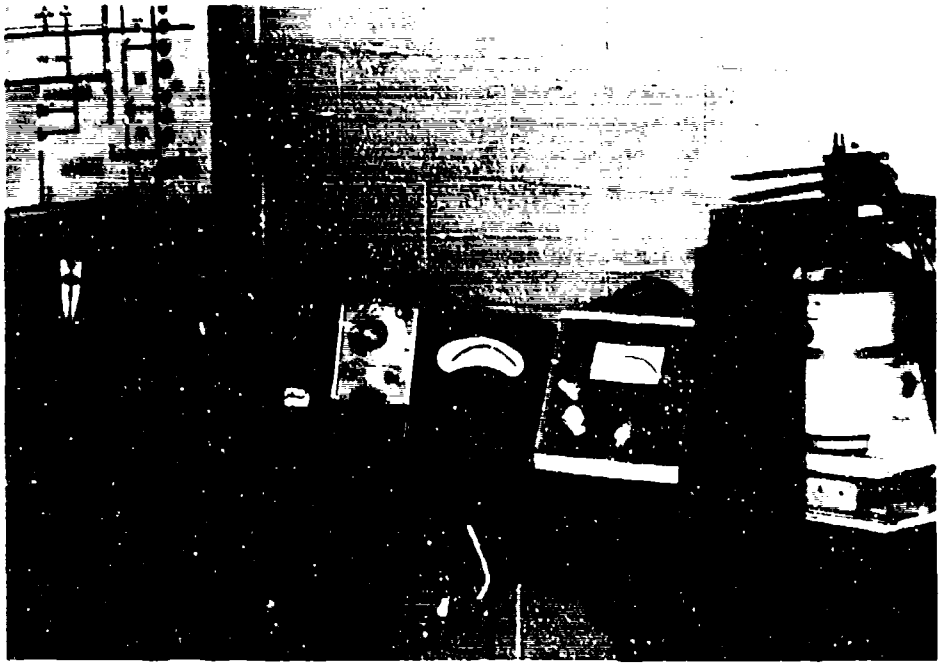

Figure 15

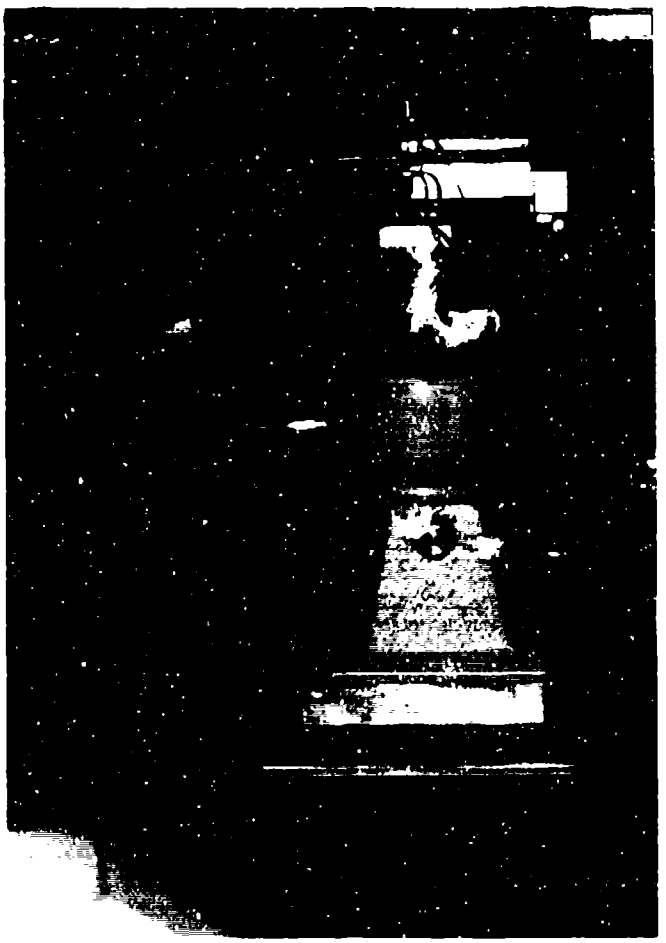

Figure 16

In order to have repeatable tests the cantilever beam must be mounted in the holder in accordance with Fig. 2 of the Appendix A which shows the re-enforced end positioned within the clamps. This position was established by means of a micrometer which measured the distance of the specimen tip from the edge to the steel mounting platform. This 7mm distance was maintained for all tests. Once the specimen was mounted and clamped, the shaker was energized and the oscillator frequency swept slowly up while observing the amplitude of the accelerometer output. The oscillator was tuned to give a minimum amplitude to the observed wave form. This is refered to as the "notch" frequency which corresponds to the first mode resonance. The dial adjustment of the oscillator is very sensitive to the touch, with the result that frequency could be adjusted to 0.5Hz as read by the frequency marker on the digital oscilloscope display. A typical micro strain and accelerometer trace is shown in Figure 17 and from these traces the peak strain and peak g's acceleration are taken for the calculation of loss factor. These traces are created for a range of amplifier output voltage from 0.5 volts to 10 volts, the maximum voltage being a fucntion of the specimen strain which, for this particular composite, should not exceed a microstrain of 1000. For each run the minum in the accelerometer output was read on the above trace, and then to get an accurate reading of the frequency, a frequency spectrum was made as shown in Figure 18.

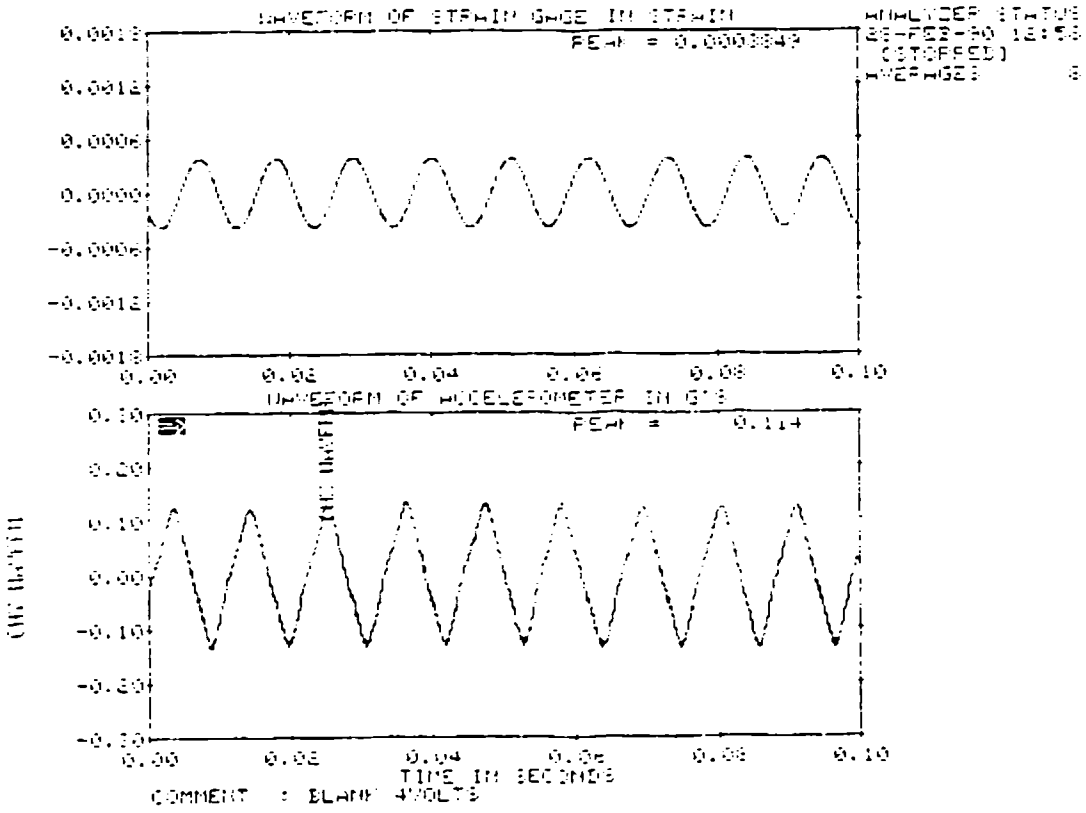

Figure 17

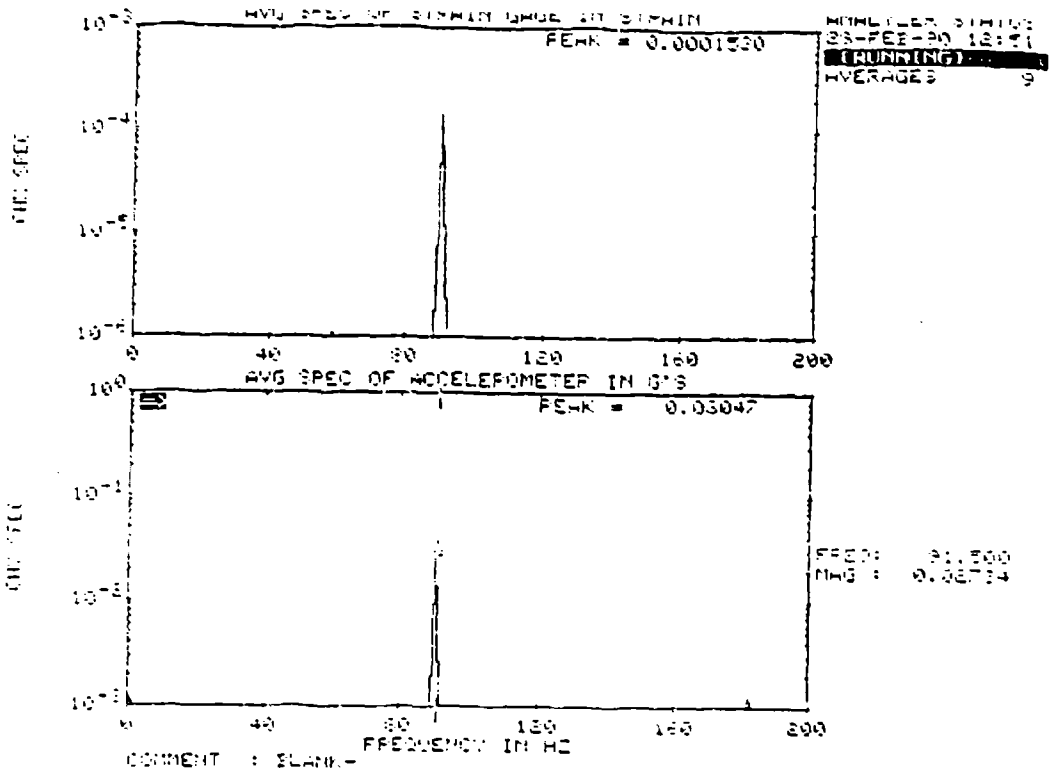

Figure 18

When the analyzer is run as a digital oscilloscope a decay curve can be obtained by statically deflecting and then releasing the cantilever specimen. This can be used to calculate a log decrement value to cross check the value of specimen loss factor calculated from the acceleration and strain energy readings. A typical decay curve is shown in Figure 19.

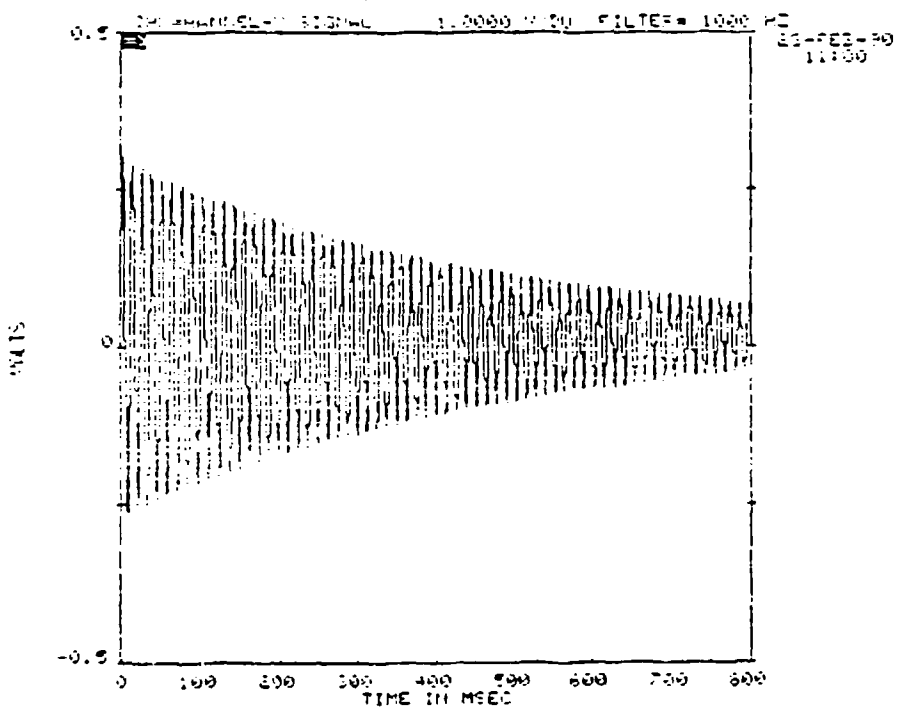

Figure 19

DATA SUMMARY:

The calculated Q from the specimen acceleration in "g's" and the root strain for both blank and composites with imbedded wires is given in the Table I. For each specimen the resonance frequency determined by tuning to the acceleration notch is given, along with the calculated modulus of elasticity and the measured density. The density γ given on the chart is calculated from the measured modulus, E, and the measured resonance frequency f_1. ζ% is the % of critical damping which is equal to loss factor/2 or 1/2Q. For perspective in conventional metallic alloy systems, when the Critical Damping % exceeds 1% the system is considered to have a useful level of damping. By this criterion, the F2015-020 samples are the only cantilever specimen tested which can be considered to possess really significant damping.

DISCUSSION OF RESULTS

Using a graphite epoxy composite matrix NiTi wires were imbedded in the outer fiber surfaces of cantilever specimen by laying up pre-preg sheets and then hot pressing the assembly. The 1"x10"samples cut from the hot pressed sheet were fitted with re-enforced ends and had strain gauges mounted at the root section of the cantilever. Two wire diameters were chosen to provide a variation in the volume % of wire in the specimen, nominally 3% and 10%. Two compositions of NiTi were chosen for passive damping experiments, one which would be martensitic at room temperature and the other beta or austenite at room temperature. In shape memory alloys, damping is due to the motion of martensite variant plate boundaries under stress, and a typical specific damping capacity for these alloys is in excess of 40%. This high damping level falls off to only 0.5 to 1% when the martensite transforms to the beta or elevated temperature phase. The alloy in the beta condition can transform to martensite when subjected to a sufficiently high stress;the magnitude of the required stress for stress induced transformation,(SIM), is a function of temperature. Obviously at the martensite transformation temperature M_s the stress required drops to zero, but rises with ΔT the difference between the ambient and the M_s. The SIM reaction is also dissipative, and when martensite forms as a result of the externally applied stress it will provide damping for the period that phase exists, a function of the stress duration or frequency. In addition to examining the level of damping which could be achieved by imbedding shape memory NiTi wires in the matrix, a second class of specimen was studied where the wire was electrically heated to cause it to transform from martensite to beta and, thereby, to explore the change is specimen
resonance frequency as a result of the large, circa 300%, change in the elastic modulus of NiTi when it undergoes transformation. The change in the cantilever beam modal response could arise from this modulus change provided it is present in sufficient volume. An alternative is to pre-strain the NiTi in the martensitic state, and then preserving the strain in the wire during the hot pressing

RESONANCE DWELL DATA FOR GRAPHITE-EPOXY SPECIMENS WITH IMBEDDED NITI WIRES GENERATED ON THE BOLT BERANEK AND NEWMAN RESONANCE DWELL APPARATUS

TABLE I

The excitation voltage refers to the output of the Crown power amplifier and is used to reset the drive amplitude of the shake-table to a duplicate level of g's acceleration. The Elastic modulus was determined by static deflection of the cantilever test specimen under a 10N load. The calculation of a typical modulus is shown in Appendix C.

SPECIMEN	BLANK = 1			TI 150-010			F2015-020-1			F2015-020-2			VT4610-1			VT4610-2		
DENSITY - lbs/in³	.0591			.0619			.0740			.0740			.0711			.0711		
% VOLUME SME	0			3.0			10.9			10.9			9.2			9.2		
ELASTIC MODULUS - psi	12×10^6			16.9×10^6			13.6×10^6			13.6×10^6			17.8×10^6			17.8×10^6		
TEST DATE / TIME	2/28/90/1251			2/22/90/1643			2/25/90/1544			3/28/90/1430			3/6/90			3/6/90		
FREQUENCY (f) - CPS	91.5			82.0			32.0			83.0			90.3			91.0		
EXCITATION VOLTAGE	a_o g's	με	Q CALC.	a_o g's	με	Q CALC.	a_o g's	με	Q CALC.	a_o g's	με	Q CALC.	a_o g's	με	Q CALC.	a_o g's	με	Q CALC.
.5				.0102	53.9	159.	.0095	98.8	155.	.0124	53.2	132.						
1.0	.0220	106.	181.	.0247	104.	127.	.0220	95.9	131.	.0278	97.1	109.	.0223	79.3	130.	.0201	84.9	157.
2.0	.0404	194.	181.	.0555	195.	106.	.0769	187.	73.2	.0939	183.	68.5	.0376	159.	155.	.0294	169.	207.
3.0	.0730	293.	151.	.0787	286.	110.	.143	269.	56.7	.155	264.	52.6	.0669	243.	133.	.0419	240.	213.
4.0	.114	385.	127.	.108	393.	110.	.235	370.	47.4	.229	348.	46.9	.106	317.	109.	.0605	312.	192.
5.0	.162	479.	110.	.147	500.	103.	.324	458.	42.6	.312	425.	42.0	.155	392.	92.5	.0886	388.	163.
6.0	.222	559.	94.7	.190	591.	93.7	.432	548.	38.2	.408	510.	38.6	.207	465.	82.1	.122	454.	138.
7.0	.297	646.	81.8	.241	677.	84.6	.534	630.	35.5	.514	589.	35.4	.264	536.	74.0	.169	523.	125.
8.0	.389	726	71.1	.311	775.	75.1	.639	703.	33.1	.621	665.	33.1	.325	601.	67.6	.227	594.	97.2
9.0	.487	806	62.2	.381	857.	67.8	.792	802.	30.5	.763	749.	30.3	.407	672.	60.4	.266	660.	92.1
10.0	.620	885	53.7	.455	931.	61.6				.894	816.	28.2	.475	730.	56.2	.301	722.	89.1
η_s LOSS FACTOR	.0055 → .019			.0063 → .016			.0065 → .033			.0076 → .035			.0077 → .018			.0069 → .011		
ζ %	.28 → .95			.32 → .80			.33 → 1.65			.38 → 1.75			.39 → .90			.32 → .55		
$K_o = \frac{2.23 \times 10^5}{f_1^2} \frac{\mu\text{strain}}{\text{g}}$	26.6			33.2			33.2			32.4			27.3			26.9		
$\gamma = \frac{29.98 \times 10^{-6} E}{f_1^2} \frac{\text{lbs}}{\text{in}^3}$	.0430			.0754			.0606			.0592			.0654			.0644		

operation by some form of external restraint, similar to the formation of pre-stressed concrete. If the wire to matrix bond is strong then heating the wire will cause a distributed stress to be generated as the wire tries to recover its shape as it transforms back to the beta phase.

As expected, damping in the basic composite is quite low at low strain levels, and then rising to a higher levels as the stress is increased, as shown in Figure 6. This rise in damping is probably due to the epoxy matrix which has some threshold stress for damping. The specimen with martensitic NiTi, ITI50 and F2015, were expected to show damping as a result of the high specific damping capacity of martensitic NiTi. The ITI50 wires were 0.010" diameter and the F2015 wires were 0.020" diameter, thus, with the same number of imbedded wires, the volume percentage of damping wires was 3% and 10% respectively. At the 3% level the damping contribution was not measurable, whereas, at 10% the damping was significant over the entire strain range of from 50 to 1000 μ-strain. The specimen with imbedded beta phase wire, VT4610, were prepared with only one volume percentage level, 9%. At the limit of permissible strain for the composite material, 1% or 1000 μ-strain, there was no observable shift in damping, and, indeed, it appears that the damping for this composite was slightly lower than for the basic graphite-epoxy; compare Figures 5 and 5. This is due to the fact that the damping of the NiTi in the beta phase at low stress is less than the composite material damping, and at 10% volume actually reduces the damping when imbedded. The ITI50 NiTi was imbedded as a continuous wire in the form of three loops. This was pre-strained and then laid up as a composite with the wire in the neutral axis. The jig to maintain the strain during hot pressing did not function properly, and as such, the wire could exhibit a modulus change on heating but not a distributed stress from the shape recovery. At 3% volume level, the modulus change was not effective by itself in changing the stiffness of the cantilever. The anticipated shift in beam mode due to the presence of a shape change induced distributed stress could not be evaluated.

CONCLUSIONS

1. During the period of this Phase I investigation it was established that martensitic shape memory wires imbedded in graphite-epoxy composites provide a substantial improvement in the damping characteristics of these materials. The threshold volumetric % level of wire for a realistic contribution to damping is 10%, and in discussions with others working on similar damping studies (2,3) it would appear that 15% or more would be desirable.

2. Although the available processing at UTRL dictated the use of graphite pre-preg tape for the preparation of composites with imbedded shape memory wire, the low viscosity of the epoxy at the temperature of hot pressing, circa 350°F, allowed shifting of the wires, and although better jigging could improve this situation, a better alternative would be to use thermoplastics with their higher viscosity; e.g. PEEK or PEK compositions. In the original proposed

effort these were considered, however the UTRL group felt that the graphite -epoxy would be a better composite to start with.

3. In experiments carried out at UTRL parallel, but not a part of this study, shape memory actuators were attached to the surface of composite beams and subjected to alternating I^2R heating and air cooling to examine the ability of such an array to induce vibrations. This ability was demonstrated, and at the same time it was apparent that the heating and cooling time of a wire would be the factor which would limit the upper attainable frequency.(4,5) An array of wires which were multiplexed, i.e. alternately heated to give a higher forcing frequency, was demonstrated. These forms of active control are interesting, but when the wires are imbedded in a composite as in the present studies, the frequency of cycling is drastically reduced by the inability of the wires to dissipate their heat. As such, active control is limited to relatively low frequency tuning of the composite by changing the internal stress state through shape recovery of a pre-strain in a NiTi wire. A change in modal response will also occur when the NiTi imbedded wires are heated to above their transformation point to effect a change in modulus. To be effective, this type of property change requires a relatively larger volume % of wires.

4. The stress levels required to cause stress induced martensite in a beta NiTi material are circa 60,000 psi. Therefore to use this phase change as a hysteretic energy absorber requires a composite material capable of sustaining this level of stress. The strain limit of 1000 μ-strain for the present composite turned out to be too low to exploit this mechanism; again an argument for the more strain tolerant thermoplastics.

5. The surface preparation of the NiTi wires by hydrofluoric-sulfuric acid descaling and etching was effective in giving good bond strength in the hot pressed composite. An alternative system of cleaning with a potentially lower cost and the elimination of toxic waste disposal problems and hygiene problems is by vapor blasting. This method, involving an aqueous jet with micron size Al_2O_3 entrained powder, gives a smooth satin finish which should have good bonding. Samples were sent to Prof. Craig Rogers at VA Poly. Inst. for evaluation.

6. The cantilever beam proved a good geometry for the evaluation of the effectiveness of various composite/NiTi assemblies. Two alternative driving methods were examined for inducing vibrations in the sample; at UTRL a piezoelectric film bonded to the specimen and driven by an external AC source, and at Memry Corp. the resonance dwell apparatus reported here. The latter

has the ability to drive a specimen to high stress levels at frequencies up to about 1000cps. Coupled with an FFT Analyzer this proved to be a very useful tool. For low amplitude and high frequency excitation the piezoelectric drive is preferred. The regime of interest in composite material damping would favor the resonance dwell method. In order to provide accurate tuning to the resonance frequency an improved oscillator with digital read-out would be helpful.

SUGGESTIONS FOR FURTHER DEVELOPMENT IN A PHASE II EFFORT:

1. As a result of a broad range of research in intelligent materials the basic constitutive equations of NiTi are well developed and the basic types of vibration control which can be effected by imbedded NiTi wires is established. All of the data generated to date have emphasized graphite-epoxy composites as the matrix material. Two important resins should be evaluated because of their superior toughness and their fabricating characteristics, PEEK, polyetheretherketone, manufactured by a wide range of companies but associated generally with Imperial Chemical Industries, Ltd (ICI) and a more recent duPont Chemical USA derivative PEK. These linear aromatic polymers may be injection molded, compression molded and extruded and have excellent flexural strength at elevated temperature combined with toughness and abrasion resistance. The PEK version has an advantage of a lower flow temperature which makes it possible to use sized glass fibers as a re-enforcing fiber; the flow temperature and viscosity of PEEK tends to degrade the sizing which reduces the bonding. It is felt that glass fiber composites should be explored as well as graphite and PAN fibers, although for general use the later may be too expensive.

2. The interrelationship between processing and properties should be developed; the variables being:

- Geometry
- SMA alloy and its form, wire or ribbon
- Composite matrix material
- Shapes, plates and curves
- Interfacial shear strength variables
- Fatigue using standard ASTM procedures

Fabrication processes should include:

- Filament winding
- Compression molding
- Hot Forming
- Hot Pressing

Properties:

- Damping: Active and Passive
- Acoustic propagation characteristics
- Structural Acoustics: Wave propagation
- Active control of modal response

Properties (Cont.)

Mechanical properties of beams and plates
Buckling characteristics of composite/SMA plates

4. Considerations of scaling from laboratory specimen size to mission oriented structures.

REFERENCES

1. Liang.C, Jia.J, Rogers.C.A. - Behavior of Shape Memory Alloy Reinforced Composite Plates PartII American Institute of Aeronautics and Astronautics 1989 Conf.Paper 89-1331-CP

2. Discussions with Prof. C.A. Rogers, Smart Materials and Smart Structures Laboratory, Virginia Polytechnic Institute

3. One-Dimensional Thermomechanical Constitutive Relations for Shape Memory Alloys: C.Liang and C.A. Rogers, report on ONR N00014-88-K-0566

   Formulation of a Laminated Shell Theory Incorporating Embedded Distributed Actuators: J.Jia and C.A.Rogers ASME Conference Proceedings On Adaptive Structures AD-Vol.15

4. Thermal and Mechanical Considerations in Using Shape Memory Alloys to Control Vibrations in Flexible Structures: A.V. Srinivasan, D.G. Cutts and L.McD. Schetky Conference on Smart Materials ASM, Indianapolis October 1989, to be published in Transactions ASM

5. Shape Memory Effect Alloys for Robotic Devices: L.McD. Schetky Robotics Age July 1984 - pp13-17

APPENDIX

A: CONSIDERATIONS IN THE MEASUREMENT OF DAMPING BY THE RESONANCE DWELL TECHNIQUE USING A CANTILEVER BEAM

B: MEASUREMENT OF SPECIMEN Q FROM FREE VIBRATION TESTS

C: LOAD-DEFLECTION MEASUREMENT OF COMPOSITE BEAM ELASTIC MODULUS

D: BASE PROPERTIES FOR THE AS4-3501-6 GRAPHITE EPOXY COMPOSITE

I. Static Considerations

In pure flexure, with cross-section b x h

$$\epsilon_{MAP}/h = \frac{6M}{Ebh^3} \tag{1}$$

a. Determination of maximum strain and elastic modulus for a cantilever with an end load, P and length, L

$$M_F = P\ell \tag{2}$$

$$\delta_E = \frac{4P\ell^3}{Ebh^3} \tag{3}$$

$$\delta_E = \frac{2}{3}\,\ell^2\left(\frac{\epsilon_{MAX}}{h}\right) \tag{4}$$

or

$$\frac{\delta_E}{\ell} = \frac{2}{3}\,\epsilon_{MAX}\,\frac{\ell}{h} \tag{5}$$

$$\epsilon_{MAX} = \frac{3}{2}\,\frac{h}{\ell}\,\frac{\delta_E}{\ell} \tag{6}$$

Relating the max. $\epsilon_{E.F.}$ to the free end deflectivity δ_E which from Eq. (3) is related to the applied load, P, by

$$\delta_E = \frac{4\ell^3}{Ebh^3}\,P \tag{3}$$

Thus, if δ_E is measured under P, the max. strain and the effective "composite" modulus of elasticity are thus determined from

$$\epsilon_{MAX} = \frac{3}{2}\,\frac{h}{\ell}\,\frac{\delta_E}{\ell} \tag{6}$$

$$E = \frac{4\ell^3}{h}\,\frac{P}{b\delta_E} \tag{3a}$$

b. Statical response for first mode excitation

The method of loading is described by

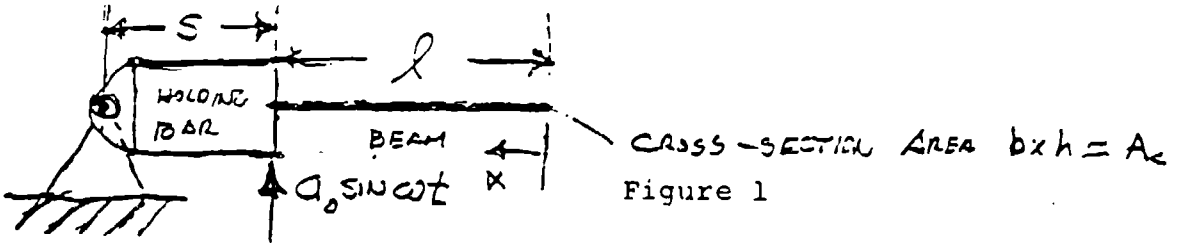

Figure 1

Thus, the beam is subjected to an acceleration distribution of amplitude

$$a(x) = a_0\left(1 - \frac{\ell - x}{s}\right) \tag{7}$$

The statical moment at $x = \ell$ is thus

$$M_\ell = \varrho\, A_c\, a_0 \int_0^\ell \left(1 - \frac{\ell - x}{s}\right)(\ell - x)\, dx \tag{8}$$

$$= \frac{\varrho\, A_c\, A_0\, \ell^2}{2}\left[1 + \frac{2}{3}\,\frac{\ell}{s}\right]$$

For which the maximum strain is given by

$$\epsilon_{MAX_\ell} = \frac{6\,M_\ell}{bh^2E} = \frac{3\,\varrho\,a_0\,\ell^2}{hE}\left[1 + \frac{2}{3}\,\frac{\ell}{s}\right]$$

or

$$= \frac{h/2\,\varrho\,A_c\,\ell^2}{hE}\,a_0\left[1 + \frac{2}{3}\,\frac{\ell}{s}\right] \tag{9}$$

Since $f_1^2 = 0.3131\,\dfrac{EI}{\varrho\,A_c\,\ell^4}$

$$\epsilon_{MAX_\ell} = 0.1566\,\frac{h}{f_1^2\,\ell^2}\,a_0\left[1 + \frac{2}{3}\,\frac{\ell}{s}\right] \tag{10}$$

and for s = 3.5 inches

$$\epsilon_{MAX_\ell} = 0.1566\,\frac{h}{f_1^2\,\ell^2}\,a_0\,[1 + 0.19\ell]$$

If a strain gauge is mounted at the root, this is the reference.

The tip deflection for this moment distribution is given by

$$w_{TIP} = \frac{\varrho\,A_c\,\ell^4}{8EI}\,a_0\left[1 + \frac{11}{15}\,\frac{\ell}{s}\right] \tag{11}$$

$$= 0.03914\,\frac{a_0}{f_1^2}\left[1 + \frac{11}{15}\,\frac{\ell}{s}\right]$$

and with s = 3.5 inches

$$= 0.03914\,\frac{a_0}{f_1^2}\left[1 + 0.209\,\frac{\ell}{s}\right]$$

is the reference for tip motion measurement in terms of double amplitude measurement

$$2\, w_{TIP} = 0.07828\, \frac{a_0}{f_1^2}\, [1 + 0.209\, \ell] \tag{11a}$$

Refer to BB&N Eq. 3

STATICAL RESPONSE FOR FIRST MODE EXCITATION

1. The method of loading previously described must be corrected for the actual position of the beam root, $x = \ell$, which does not coincide with the point of excited measurement(s) as shown

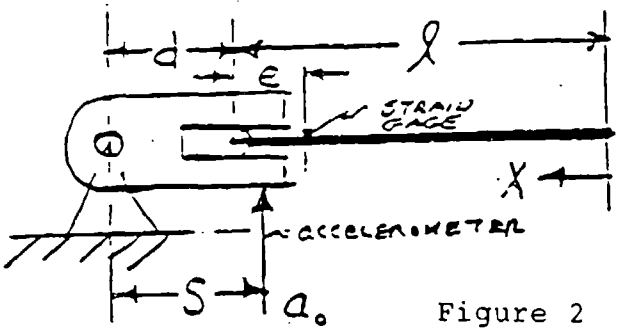

Figure 2

The corrected beam acceleration becomes

$$a(x) = a_0 \frac{d}{s} \left(1 + \frac{\ell - x}{d} \right) \tag{7c}$$

2. Additionally, since the strain is measured at some distance, e, short of the root, as shown, the moment at the point $x = \ell - e$ is required. Thus.

$$M_{\ell-e} = \varrho A_c A_0 \frac{d}{s} \int_0^{\ell-e} \left(1 + \frac{\ell - x}{d} \right) (\ell - e - x)\, dx \tag{8c}$$

$$= \frac{\varrho A_c a_0 \frac{d}{s} (\ell^2 - e^2)}{2} \left[\left(1 + \frac{2(\ell - e}{3d} \right) \left(1 - \frac{e}{2(\ell + e)} \right) - \frac{3e}{2(\ell - e)} \right]$$

As a result, Eq. (10c) provides the maximum strain at $x = \ell - e$ and is given by

$$\epsilon_{MAX_{x=\ell-e}} = 0.1566 \frac{h}{f_1^2 \ell^2} a_0 \frac{d}{s} \frac{(\ell^2 - e^2)}{\ell^2} \left[\left(1 + \frac{2(\ell - e)}{3d} \right) \left(1 - \frac{e}{2(\ell + e)} \right) - \frac{3e}{2(\ell + e)} \right] \quad (10c)$$

For: $s = 3.69$ inches
$\ell = 8.27$ inches
$d = 3.44$ inches
$e = 0.590 \pm 0.04$ inches
$h = 0.118$ inches
$b = 1.00$ inches

Note: $\ell + d = 11.71$ inches

METHOD OF ROOT DETERMINATION:

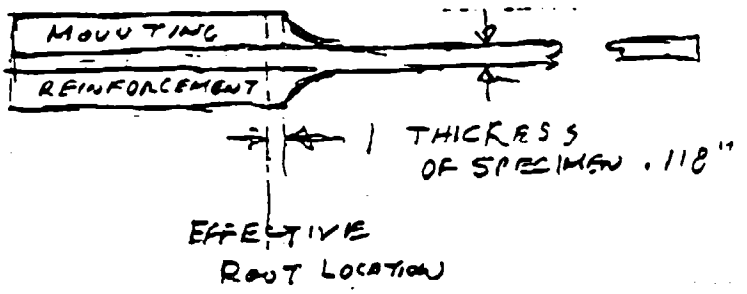

Figure 3

$$\epsilon_{MAX_{x=\ell-e}} = 5.778 \times 10^{-4} \frac{a_0}{f_1^2}$$

$$= \frac{0.2230}{f_1^2} \frac{a_0}{\text{"g"}}$$

$$= \frac{0.2230}{f_1^2} \bar{a}_0$$

where $\bar{a}_0$ is the acceleration in standard gravity units, ("g"'s).

Thus, the statical strain obtained in the extreme fiber at the location $x = \ell - e$ is related to the acceleration in "g"'s observed in the "rigid" mounting at a distance "s" from the pivot by

$$K_0 = \frac{0.2230}{f_1^2} \quad \text{strain/ "g"}$$

or

$$= \frac{2.230 \times 10^5}{f_1^2} \quad \mu\text{-strain/ "g"}$$

II. Dynamic Considerations

Undamped normal modes and frequencies

The general equation for dynamic equilibrium is

$$EI \frac{\partial^4 w}{\partial x^4} = -\varrho A_c \frac{\partial^2 w}{\partial x^2} + q(t) \tag{12}$$

For the homogeneous case $q(t) = 0$

$$w = (A \sin \alpha x + B \cos \alpha x + C \sinh \alpha x + D \cosh \alpha x) + (E \sin pt + F \cos pt) \tag{13}$$

$$\therefore \quad \frac{-\varrho A}{EI} p^2 (A \sin \alpha x + B \cos \alpha x + C \sinh \alpha x + D \cosh \alpha x) \sin pt$$

$$+ \alpha^4 (A \sin \alpha x + B \cos \alpha x + C \sinh \alpha x + D \cosh \alpha x) \sin pt \equiv 0$$

or

$$\frac{\alpha^4}{p^2} = \frac{\varrho A_c}{EI}$$

To satisfy the B.C. for a cantilever

$$\text{at the fixed end} \quad w = 0$$

$$x = 0 \quad \frac{\partial w}{\partial x} = 0 \tag{14}$$

$$\text{at the free end} \quad \frac{\partial^2 w}{\partial x^2} = 0 \quad (M = 0)$$

$$x = \ell \quad \frac{\partial^3 w}{\partial x^3} = 0 \quad (V = 0) \tag{15}$$

fro, (14)

$$B + D = 0 \tag{14a}$$

$$A + C = 0 \tag{14b}$$

from (15)

$$-A \sin \alpha\ell - B \cos \alpha\ell + C \sinh \alpha\ell + D \cosh \alpha\ell = 0 \tag{15a}$$

$$-A \cos \alpha\ell + B \sin \alpha\ell + C \cosh \alpha\ell + D \sinh \alpha\ell = 0 \tag{15b}$$

using (14)

$$-A (\sin \alpha\ell + \sinh \alpha\ell) - B (\cos \alpha\ell - \cosh \alpha\ell) = 0 \tag{15c}$$

$$-A (\cos \alpha\ell + \cosh \alpha\ell) + B (\sin \alpha\ell - \sinh \alpha\ell) = 0 \tag{15d}$$

which requires

$$-(\sin \alpha\ell + \sinh \alpha\ell) - \frac{(\cos \alpha\ell + \cos \alpha\ell)^2}{\sin \alpha\ell - \sinh \alpha\ell} = 0$$

or

$$\begin{aligned} -\sin^2 \alpha\ell + \sinh^2 \alpha\ell - (\cos \alpha\ell + \cosh \alpha\ell)^2 &= 0 \\ -(\sin^2 \alpha\ell + \cos^2 \alpha\ell) + (\sinh^2 \alpha\ell - \cosh^2 \alpha\ell) - 2 \cos \alpha\ell \cosh \alpha\ell &= 0 \\ -1 \qquad\qquad -1 \qquad\qquad - 2 \cos \alpha\ell \cosh \alpha\ell &= 0 \end{aligned} \tag{16}$$

or,

$$\cos \alpha\ell = \frac{-1}{\cosh \alpha\ell} \tag{16a}$$

for which the first root is

$$a_1\ell = 1.875 \tag{17}$$

and

$$a_1 = \frac{1.875}{\ell} \tag{17a}$$

Hence

$$p_1 = a_1^2 \sqrt{\frac{EI}{\varrho A_c}} = \frac{3.516}{\ell^2} \sqrt{\frac{EI}{\varrho A_c}} \quad \text{Frequency} \tag{18}$$

Subsequently, roots yield

$$p_2 = 22.03\,\ell^{-2}\sqrt{\frac{EI}{\varrho\,A_c}}$$

$$p_3 = 61.70\,\ell^{-2}\sqrt{\frac{EI}{\varrho\,A_c}} \qquad (19)$$

$$p_4 = 120.9\,\ell^{-2}\sqrt{\frac{EI}{\varrho\,A_c}}$$

From (15c)

$$B_M = -A_M\,\frac{\sin a_M\ell + \sinh a_M\ell}{\cos a_M\ell + \cosh a_M\ell} = -f\,T\,(a_m\ell) \qquad (20)$$

Whence,

$$w = A_M\,[\sin a_M x - T\,(a_M\ell)\cos a_M x - \sinh a_M x + T\cosh a_M x]\sin\sqrt{\frac{EI}{\varrho\,A_c}}\,a_M^2\,t$$

$$+ B_M\,[\quad \text{ditto} \quad]\cos\sqrt{\frac{EI}{\varrho\,A_c}}\,a_M^2 t \qquad (21)^*$$

$$\frac{\partial^2 w}{\partial x^2} = A_M\,a_M^2\,[-\sin a_M x + T\,(a_M\ell)\cos aa_M x - \sinh a_M x = T\,(a_M\ell)\cos a_M x]\ \sin p_n t \quad \text{etc.} \qquad (22)^*$$

* Note that the terms in [ ] in Eqs. (21) and (22) are the mode shapes for displacement and bending moment (fiber stress) respectively.

Thus, at $x = 0$, the fixed end

$$M_0 = 2A_1 \alpha_M^2 T(\alpha_M \ell) EI$$

$$\text{for } M = 1,\ \alpha_1 \ell = 1.875 \tag{23}$$

$$T(\alpha_1 \ell) = 1.3622$$

$$M_0 = 9.578\, A_1 \frac{EI}{\ell^2} \tag{24}$$

and at $x = \ell$ the free end

$$w_\ell = 2.724\, A_1 \tag{25}$$

Thus,

$$M_0 = 3.516\, w_\ell \frac{EI}{\ell^2} \text{ for 1st mode operation} \tag{26}$$

$$\sigma_0 = \frac{h}{2I} M_0 = 1.758\, w_\ell \frac{Eh}{\ell^2} \tag{27}$$

III. Damping Considerations

Define the following energy quantities associated with damped vibration

L	=	total energy absorbed by damping/cycle
$D(\sigma)$	=	specific damping energy of the material as a function of stress
$D_M(\sigma_M)$	=	specific damping energy at the maximum stages σ_M in the species
V_0	=	total volume of the specimen
V	=	total volume of the specimen
σ	=	amplitude of reversing stress
U	=	strain energy at max. amplitude

$$L = \int_0^{V_0} D \, dV \tag{28}$$

$$= D_M V_0 \int_0^1 \frac{D}{D_M} \, d\left(\frac{V}{V_0}\right) = D_M \, V_0 \, \alpha$$

$$U = \int_0^{V_0} \frac{\sigma^2}{2E} \, dV \tag{29}$$

$$= \frac{\sigma_M^2 \, V_0}{2E} \int_0^1 \left(\frac{\sigma}{\sigma_M}\right)^2 d\left(\frac{V}{V_0}\right) = \frac{\sigma_M^2}{2E} \, V_0 \, \beta$$

In addition, there are the following defined quantities

$$\eta_s = \frac{L}{2\pi U} \quad , \quad \text{specimen loss factor} \tag{30}$$

$$= \frac{E}{\pi} \frac{D_u}{\sigma_M^2} \frac{\alpha}{\beta} \quad \text{from Eq. (28) and (29)}$$

$$\eta = \frac{E}{\pi} \frac{D_M}{\sigma_M^2} \quad , \quad \text{material loss factor at constant stress } \sigma_M \tag{31}$$

$$= \eta_s \frac{\beta}{\alpha}$$

$$\delta_s = -\log\left[\frac{A_{NH}}{A_N}\right], \quad \text{specimen log decrement} \tag{32}$$

$$B_s = \frac{\Delta\omega_s}{\sqrt{3}\ P_M}, \quad \text{specimen bandwidth at 1/2 peak amplitude at frequency of mode M, } P_M \tag{33}$$

$$= \eta_s$$

$$\psi = 2\pi\,\eta, \quad \text{material dampling capacity} \tag{34}$$

$$\psi_s = 2\pi\,\eta_s \quad \text{specimen damping capacity} \tag{35}$$

$$= 2\,\delta_s$$

$$Q_s = \frac{A_{RESONANT}}{A_{STATICAL}} \quad \text{Peak intensity or magnification ratio} \tag{36}$$

$$= \frac{1}{\eta_s}$$

A_{RES} = Amplitude at resonance

$A_{STATICAL}$ = Amplitude resulting loading from loading of same amplitude applied statically

Referring to BB&N's Manual

$$g_s = \eta_s \tag{37}$$

$$C_1 = \eta \tag{38}$$

$$= g_s \frac{\beta}{a} \tag{39}$$

or

$$= g_s \frac{\int_0^1 \left(\frac{\sigma}{\sigma_M}\right)^2 d\left(\frac{V}{V_0}\right)}{\int_0^1 \frac{D}{D_M}\, d\left(\frac{V}{V_0}\right)} \tag{40}$$

Assuming, Eq. (40), $D = J\,\sigma^N$

Then

$$a = \int_0^1 \frac{D}{D_M}\, d\left(\frac{V}{V_0}\right) = \int_0^1 \left(\frac{\sigma}{\sigma_M}\right)^N d\left(\frac{V}{V_0}\right) \tag{41}$$

Noting that the moment mode shape ϕ_j, is given by Eq. (22) within [ ] or

$$\phi_j = [-\sin a_j x + T(a_j \ell) \cos a_j x - \sinh a_j x + T(a_j \ell) \cosh a_j] \tag{42}$$

where $a_j = \frac{\lambda_j}{\ell}$, thus $\frac{\lambda_j x}{\ell} = z$ for $0 < z < \lambda_j$

Equally well, one can divide through by the constant $T(\lambda_M)$ to obtain the form coincident with BB&N Eq. (5)

$$\phi_j(z) = \left[\cos z + \cosh z - \frac{1}{T(\lambda_j)} (\sin z + \sinh z)\right] \tag{43}$$

where

$$\frac{1}{T(\lambda_j)} = \frac{\cos \lambda_j + \cosh \lambda_j}{\sin \lambda_j + \sinh \lambda_j} \quad \text{from Eq. (20)}$$

Thus, for the first mode $j = 1$ with $\sigma = \frac{M_y}{I}$

$$\frac{\sigma}{\sigma_M} = \frac{\phi_1(z)\, y}{\phi_1(0)\, h/2} = \frac{\phi_1(z)}{2} \left(\frac{y}{\frac{h}{2}}\right) \tag{44}$$

now

$$\int_0^1 \frac{\phi_1^N(z)}{2^N} \left(\frac{y}{\frac{h}{2}}\right)^N d\left(\frac{V}{V_0}\right) = \frac{1}{2^N} \int_0^\lambda \int_0^1 \phi_1^N(z)\, Y^N\, dY\, dz \tag{45}$$

for constant width b with $Y = y/h/2$

Thus,

$$a = \frac{1}{2^N (N + 1)} \int_0^{\lambda} \phi_1^N (z)\, dz \tag{46}$$

Similarly,

$$\beta = \frac{1}{2^3 (3)} \int_0^{\lambda} \phi_1^2 (z)\, dz \tag{47}$$

or

$$\eta = \eta_s \frac{\beta}{a} \tag{48}$$

$$= \frac{2^{N-2}(N + 1)}{3} \frac{\int_0^{\lambda} \phi_1^2 (z)\, dz}{\int_0^{\lambda} \phi_1^N (z)\, dz}$$

Referring to B,B&N (Eq. 4&5a), if N - 2 = n, then

$$\eta = \eta_s \frac{2^n (n + 3)}{3} \frac{\int_0^{\lambda} \phi_1^2 (z)\, dz}{\int_0^{\lambda} \phi^{n+2} (z)\, dz} \tag{49}$$

Note that from Eq. (30) with $D = J \sigma^N$

$$\eta_s = \frac{E}{\pi} J \frac{\sigma_M^N}{\sigma_M^2} \tag{50}$$

$$= C \sigma_M^{N-2}$$

Hence

$$N - 2 = \frac{\log (\eta_{s_1}/\eta_{s_2})}{\log (\sigma_1/\sigma_2)} \tag{51}$$

or

$$= n$$

See B,B&N Eq. 7.

Evaluation of Integrals in First Mode with n = .5

Sta	ϕ (z)	$\phi^{2.5}$ (z)	SM	f (β)	ϕ^2	SM	f (α)
0	2.000	5.6568	1	5.6568	4	1	4
1	1.7214	3.8878	4		2.9632	4	
2	1.4442	2.5065	2		2.0857	2	
3	1.1817	1.5180	4		1.3964	4	
4	0.9223	0.8169	2		0.8506	2	
5	0.6790	0.3799	4		0.4610	4	
6	0.4598	0.1434	2		0.2114	2	
7	0.2729	0.03891	4		0.07447	4	
8	0.1277	0.005827	2		0.01631	2	
9	0.0335	0.000205	4		0.001122	4	
10	0	0	1		0	1	
				Σ = 35.90			Σ = 29.91

λ = 1.8751

B_1 = 0.7341

$$\beta' = \frac{0.1\lambda}{3} \Sigma f(\beta) = 2.2439$$

$$\alpha' = \frac{0.1\lambda}{3} \Sigma f(\alpha) = 1.8696$$

Thus

$$R_1 = \frac{3}{(3.5)(2)^5} \frac{2.2439}{1.8696} = 0.7274$$

Compare B,B&N (page 9) R_1 = 0.728

B: MEASUREMENT OF THE SPECIMEN Q FROM FREE VIBRATION TESTS.

The damped wave form shown in Figure 19 can be used to calculate the apparent resonance frequency of the beam as well as its Q. The relationships between log decrement, specific damping capacity, and material damping capacity are shown on page 13 of Appendix A. The calculation of log decrement δ_s, specimen bandwidth η_s, and Q from the free vibration decay is given below for specimens F2015-020-#1 and for VT4610-#2.

F2015-020-#1

Cycle #	Amplitude	μ-Strain	δ_s	η_s	Q
2	3.50	102	.0311	.00991	92.4
6	3.09	90.2	.0319	.01010	98.5
10	2.72		.0292	.00930	108
14	2.42		.0254	.00809	124
16	2.30	67.1			
Overall 2-16			.0300	.00955	105

Observed No of Cycle "peaks" in 200μsec frame=16

Computed Frequency = 15.9/.200 = 79.5 cps
Scale factor 2.45" = 0.5volts=143μ-strain

VT4610-#2

2	2.70	158	.0263	.00838	119
6	2.43		.0237	.00755	132
10	2.21		.0225	.00715	140
14	2.02		.0206	.00657	152
18	1.86	109			
Overall 2-18			.0233	.00741	135

Observed No of Cycle "peaks" on 200μsec frame=18.8
Computed Frequency = 17.8/.200 = 89.0cps
Scale Factor: 2.45" = 1volt=286μ-strain

The calculated Q's agree reasonably well with the Q's from the resonance dwell data. The frequency is off by 2 to 3 cps which is attributed to the difficulty of making a very fine adjustment in the frequency of the oscillator in tuning for the notch frequency. A digital oscillator would be desirable for future experiments.

C: LOAD -DEFLECTION MEASUREMENT OF COMPOSITE BEAM ELASTIC MODULUS

In order to convert the strain reading of the cantilever specimen into stress, it was necessary to measure the beam modulus for each configuration since the modulus departs from the value for the blank as a function of the imbedded wire volume percent.

The cantilever specimen was clamped in a rigid manner and the tip deflection measured when a 10N precision weight was hung from the end. The deflection was measured with a dial gauge, and the strain output of the strain gauge was measured using the same bridge used in the dynamic tests.

Sample Calculations: Sample F2015-020, values for the other beams are shown on the summary data sheet.

Distance from free edge to load and dial indicator gauge = 5 mm
Distance from Load point to the strain gauge = 189 mm
Distance from Load point to fixed end = 205 mm

Cross Section: width(b) = 25.48 mm
thickness(h) = 2.96 mm

LOAD	DIAL INDICATOR READING	DEFLECTION mm	μ-STRAIN (Gauge)
10N	561		520
0	1128	5.67*	
10N	574		520
0	1129	5.55	
10N	574		520
0	1127	5.53	
		Average 5.54	

* neglected reading

Calculated Strain at the Gauge:

$$\epsilon_G = [(1.5)\frac{2.96}{205^2}(5.54)]\frac{189}{205} = 0.000540$$

Calculated Modulus:

$$E = 4\left(\frac{205}{2.96}\right)^3\left[\frac{10}{(25.48)(5.54)}\right] = 94,132 N/mm^2 = 13.6 x 10^3 ksi$$

D: BASE PROPERTIES FOR THE AS4-3501-6 GRAPHITE EPOXY COMPOSITE

Properties given in CenBASE/Material
Volume 3 - Thermosets, Elastomers, Composites
Films, Fibers & Metals
John Wiley & Sons 1990

Unii-Tape Graphite Epoxy

Type ASI

Tensile Modulus $20 \times 10_6$ psi

Tensile Strength 310 KSI

Cured Ply Thickness 0.005"

Cure Temperature 350°F

62% Fiber Fill

Cure Pressure 50 psi

Flexural Strength 260 KSI